This article has been accepted for publication in IEEE Wireless Communications Letters. This is the author's version which has not been fully edited and content may change prior to final publication. Citation information: DOI 10.1109/LWC.2025.3576010

`SCOPE`: Cooperative Integrated Communications and Sensing for Material Classification at Sub-Terahertz Frequencies

Khandaker Foysal Haque, Xavier Cantos-Roman, Francesca Meneghello,
Josep Miquel Jornet and Francesco Restuccia

***Abstract*—In this letter, we propose `SCOPE`—a novel, entropy-weighted ensembling approach for material classification at sub-Terahertz (THz) frequencies. Unlike existing methods that primarily use dedicated radars, `SCOPE` builds upon an integrated communication and sensing system and leverages information from both penetrating and reflected signals to enhance spatial resolution and detection accuracy across environments. We adopted spatial variability augmentation (SVA) to address the challenge of generalization across varying transmission distances and antenna gains. While most prior works are limited to radar systems or simulations, `SCOPE` is implemented and validated in a real sub-THz system working with a 10 GHz bandwidth. Our assessments across different sensing distances, antenna gains, and channel conditions demonstrate the efficacy of `SCOPE`, which reaches up to 99% accuracy in detecting five materials—glass, wood, metal, air, and plastic—outperforming existing techniques. To facilitate reproducibility, our dataset and code are available at: https://github.com/kfoysalhaque/SCOPE.**

I. INTRODUCTION

The sub-Terahertz (THz) band (0.1–0.3 THz) is emerging as a key resource for future communication and sensing systems. The sub-THz spectrum offers a practical balance between bandwidth availability and manageable propagation effects, enabling high-data-rate communications and precise wireless sensing. It is particularly suited for high-resolution sensing applications—such as environmental mapping, security screening, and material classification—that demand fine-grained sensing data collection, which lower-frequency systems cannot provide [1]. However, the adoption of sub-THz frequencies for sensing has been limited, with most approaches relying on dedicated radars [1], [2]. Material classification using radar and mmWave sensing has been widely explored for applications such as security screening, industrial automation, and biomedical sensing. Traditional methods, such as infrared spectroscopy and X-ray diffraction, offer high accuracy but require controlled scenarios and specialized hardware, limiting their deployability [2]. Several studies have investigated machine learning and deep learning techniques for mmWave radar-based material classification. Skaria et al. applied CNN-based feature extraction to mmWave radar sensor data for this purpose [1]. Similarly, Weiss et al. demonstrated 60-GHz radar-based material classification using deep convolutional neural networks (DCNNs), achieving promising results in controlled environments [2]. He et al. explored contact-free material recognition with mmWave radar, employing spatial enhancement and frequency-domain processing [3]. Additionally, Khushaba and Hill investigated wavelet scattering transforms for radar-based material differentiation, comparing centimeter-wave and millimeter-wave radar units to assess their classification capabilities across different frequency ranges, highlighting trade-offs between robustness and resolution [4]. However, these approaches remain standalone sensing techniques, often relying on pre-trained models that lack adaptability in dynamic environments.

Despite these advancements, existing methods face four critical limitations. First, most radar-based approaches operate independently of communication systems, failing to leverage integrated sensing and communication (ISAC) frameworks. Second, they predominantly rely on reflected signals, overlooking penetrating signals, which can provide valuable material-dependent features. Third, generalization across transmission distances and antenna gains has not been extensively studied, limiting robustness in practical scenarios. Fourth, most prior works focus on mmWave frequencies, whereas our proposed SCOPE framework operates in the sub-THz band at 130 GHz with 10 GHz of bandwidth, offering finer resolution and enhanced material classification capabilities.

To address these limitations, we propose `SCOPE`, a sub-THz integrated communication and sensing framework operating at 130 GHz with a 10 GHz bandwidth, specifically designed for high-precision material identification. Unlike conventional radar-based approaches, `SCOPE` leverages the channel frequency response (CFR) from both penetrating and reflected signals through an entropy-weighted ensembling technique, enhancing spatial resolution and material detection by utilizing distinct features from each signal path.

Summary of Contributions:

- We develop `SCOPE`, the first sub-THz integrated communication and sensing system for material classification. Through entropy-weighted ensembling, it dynamically integrates penetrating and reflected signal components, enabling fine-grained feature extraction and precise material identification.
- We introduce spatial variability augmentation (SVA) to improve the system's ability to generalize across diverse transmission distances and antenna gains, achieving up to a 63.6% improvement in accuracy across distance variations and a 24–27% accuracy increase for different antenna gains.
- We rigorously evaluate `SCOPE` on the TeraNova testbed [5] through extensive real-world experiments, achieving up to 99% accuracy in detecting materials such as glass, wood, metal, plastic, and air. We provide open-source access to our dataset and code to facilitate further research.

II. `SCOPE`: SUB-THZ PRECISION SENSING SYSTEM

At sub-THz frequencies, signals fully penetrate transparent materials (e.g., air) but reflect off dense ones (e.g., metal), while materials like wood or glass exhibit both behaviors. `SCOPE` employs an entropy-based ensembling approach to

---

K. F. Haque, X. Cantos-Roman, J. M. Jornet and F. Restuccia are with the Institute for the Wireless Internet of Things, Northeastern University, United States. F. Meneghello is with the Dept. of Information Engineering, University of Padova, Italy. Corresponding author email: haque.k@northeastern.edu. This work has been supported in part by the National Science Foundation under grants CNS-2134973, CNS-2225590, and ECCS-2229472; by the Air Force Office of Scientific Research under grant FA9550-23-1-0261; and by the Office of Naval Research under grant N00014-23-1-2221. The U.S. Government is authorized to reproduce and distribute reprints for governmental purposes notwithstanding any copyright notation. The views expressed are those of the authors and do not necessarily reflect the official policies or endorsements of the U.S. Air Force, U.S. Navy, or the U.S. Government.

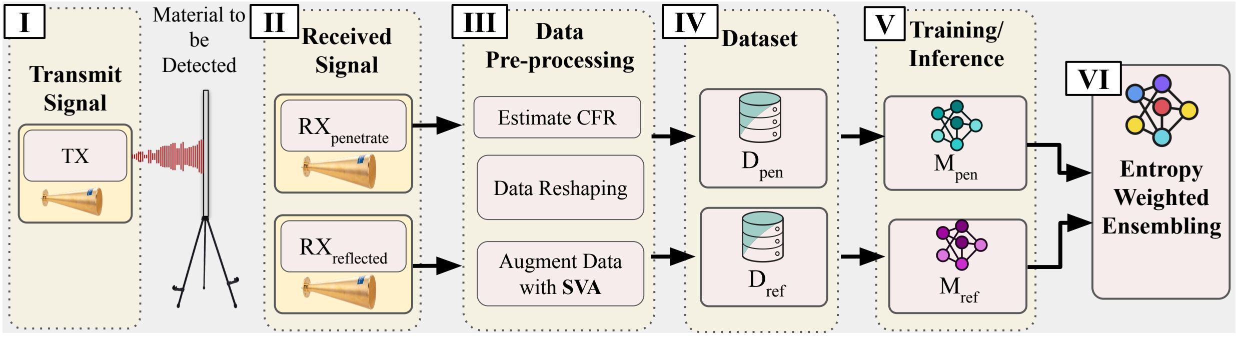

Fig. 1: A walkthrough of `SCOPE`

leverage CFR from both penetrating and reflected signals, enhancing material detection and characterization.

A. `SCOPE` System Model

In this study, we employ a Linear Frequency Modulated (LFM) pulse, commonly known as a chirp, as the transmitted signal. An LFM pulse is characterized by a frequency that varies linearly over time within the pulse duration. Mathematically, the transmitted signal $s(t)$ can be written as

$$s(t) = A \cdot \exp\left(j2\pi\left(f_0 t + \frac{K}{2}t^2\right)\right), \quad 0 \le t \le T, \tag{1}$$

where t is the time index, A and f_0 are the amplitude and the starting frequency of the chirp respectively, and $K = B/T$ is the chirp rate, with bandwidth B and pulse duration T. This choice is motivated by the high-resolution sensing and efficient communication requirements of `SCOPE` [6]. The wide bandwidth of LFM pulses enables high-range resolution, allowing precise estimation of material properties. The linear frequency variation provides resilience against Doppler shifts from relative motion, enabling sensing in dynamic environments. Furthermore, an LFM pulse can also be modulated to carry communication information, making it highly suitable for integrated sensing and communication (ISAC) applications. In particular, Chirp-Spread M-ary Phase Shift Keying (CS-MPSK) leverages the inherent structure of the LFM waveform to support simultaneous communication and sensing without requiring additional spectral resources [7]. By embedding data into the chirp waveform using M-ary PSK, CS-MPSK allows the same transmitted signal to be used for material classification while maintaining efficient communication performance, reinforcing the viability of LFM-based ISAC. While CS-MPSK modulation is not experimentally implemented in this study, the theoretical compatibility of the LFM pulse with such schemes underscores its versatility and potential for advancing integrated communication and sensing systems at sub-THz and THz frequencies.

1) Channel Estimation: To achieve time synchronization at the receiver, we cross-correlate the received signal $r(t)$ with the transmitted chirp signal $s(t)$, leveraging the chirp's sharp autocorrelation peak for accurate alignment. This process ensures that the received and transmitted signals are precisely synchronized in time. Once synchronized, we estimate the CFR as $R(k)/S(k)$, where $R(k) = \mathcal{F}\{r(t)\}$ and $S(k) = \mathcal{F}\{s(t)\}$ are the fast Fourier transforms (FFTs) of the synchronized received and transmitted signals, respectively, with $k \in \{0, N-1\}$ representing the frequency bin index. In `SCOPE`, the CFR serves as the core sensing primitive, capturing material-induced reflections, transmissions, and scattering effects. While CFR is primarily used for material classification, it also provides critical channel information for communication. In ISAC systems, the estimated CFR facilitates dynamic transmission adaptation, enabling techniques such as beamforming optimization, power control, and waveform selection. By continuously monitoring CFR variations, `SCOPE` enhances both sensing accuracy and communication reliability, establishing a unified ISAC framework.

2) `SCOPE` Walkthrough: Figure 1 illustrates the main steps of the `SCOPE` cooperative and integrated sensing approach. The system consists of a sub-THz transmitter and two sub-THz receivers, one of which collects the signal that penetrates through the material while the other collects the reflected signal. The material to be identified is interposed between the transmitter and the receiver measuring the penetrating signal. The second receiver is placed on the same side as the transmitter. Depending on the material properties, the transmitted signal (Step I) either penetrates through the object, reflects off the surface, or both, and is subsequently received by the sub-THz receivers (Step II). The received signal is then down-converted, synchronized (see Section II-A), and demodulated. Hence, the data is passed through the data pre-processing block (Step III in Figure 1) consisting of three main steps—channel estimation, data reshaping, and data augmentation. The CFR is first obtained as presented in Section II-A1. To reduce the computational complexity of the learning algorithm, Principal Component Analysis (PCA) is applied to the N-dimensional complex vector, reducing its dimensionality to N'. Specifically, starting from $N = 160,000$ elements, PCA allows reducing the relevant components to $N' = 20,000$, squeezing N by more than 87.5%, while retaining 95% of the variance. The reduced vector is then reshaped into a three-dimensional tensor of size $n \times n \times c$, where $n = \text{int}(\sqrt{N'})$ and $c = 2$, representing the real and imaginary components of the complex samples. For our learning algorithm (see Section II-C), which is based on three VGG blocks, this transformation reduces the computational complexity by approximately 50%, enabling efficient processing while preserving critical frequency-domain features. Next, the CFR vectors representing both the penetrating and reflected channels are augmented using the SVA approach presented in Section II-B to help the model learn variations linked with different transmission distances and antenna gains. Indeed, while the data captured on the oscilloscope represents

This article has been accepted for publication in IEEE Wireless Communications Letters. This is the author's version which has not been fully edited and content may change prior to final publication. Citation information: DOI 10.1109/LWC.2025.3576010

real signals, they are inherently linked with the experimental conditions, such as specific transmission distances and antenna configurations. SVA mitigates this limitation by simulating spatial variations that naturally occur in practical deployments, enriching the dataset while preserving the fundamental characteristics of the signals. This augmentation ensures that the training dataset contains more diverse realistic conditions, enabling the model to learn a more robust feature space that improves online classification performance. The original data along with the augmented data create two datasets—D_{pen} and D_{ref} for penetrating and reflected signals respectively (Step IV in Figure 1). Two separate convolutional neural network (CNN)-based feature extractors (described in Section II-C) are trained on these datasets, obtaining a penetrating model M_{pen} and a reflected model M_{ref} (Step V). During inference, these models independently produce probability distributions over the possible material classes. These probabilities are passed through the entropy-weighted-ensembling block which combines the outputs from both models, ensuring that the final prediction takes into account both penetrating and reflected signal characteristics, weighing more the more confident model (Step VI, see Section II-D).

B. SVA for Sub-THz Material Detection

Distance Scaling for Path Loss and Phase Shift. This approach applies path loss and phase adjustments independently to the CFRs associated with the penetrating and reflected signals, capturing the specific ways each signal is affected by propagation.

The path loss represents the reduction in signal strength as the wave propagates from the transmitter to the receiver. In this study, we model path loss using the log-distance equation $L(d) = L_0 + 10n \log_{10}\left(\frac{d}{d_0}\right)$, where L_0 is the path loss at a reference distance d_0 and n is the path loss exponent, which characterizes the rate of signal attenuation. Sen et al. provide an extensive empirical study on sub-THz indoor line-of-sight propagation, demonstrating its effectiveness in accurately characterizing real-world channel behavior [8].

Considering this model, the CFR magnitude is adjusted for both penetrating and reflected signals using

$$\begin{aligned} |\text{CFR}_{\text{pen}}(d)| &= |\text{CFR}_{\text{pen}}(d_0)| \cdot 10^{-\frac{L(d)-L_0}{20}}, \\ |\text{CFR}_{\text{ref}}(d)| &= |\text{CFR}_{\text{ref}}(d_0)| \cdot 10^{-\frac{L(d)-L_0}{20}}. \end{aligned} \tag{2}$$

The adjustment factor $10^{-\frac{L(d)-L_0}{20}}$ scales the CFR magnitude to reflect the amplitude attenuation due to the path loss. The factor is derived from the path loss expression and the division by 20 is because the CFR magnitude represents signal amplitude, which is proportional to the square root of power.

In addition to the path loss, the transmitted signal undergoes a phase shift as the wavefront propagates. This causes a change in the phase of the CFR. For a target distance d, the phase shift $\Delta\phi$ is approximated as $\Delta\phi = \frac{2\pi d}{\lambda}$. Although this assumes a far-field planar wave, it reasonably approximates near-field conditions as long as the target distance $d < \frac{2D^2}{\lambda}$. The phase-adjusted penetrating and reflected CFR is obtained as

$$\begin{aligned} \text{CFR}_{\text{pen}}(d) &= |\text{CFR}_{\text{pen}}(d)| \cdot e^{j(\angle \text{CFR}_{\text{pen}}(d_0) + \Delta\phi)}, \\ \text{CFR}_{\text{ref}}(d) &= |\text{CFR}_{\text{ref}}(d)| \cdot e^{j(\angle \text{CFR}_{\text{ref}}(d_0) + \Delta\phi)}. \end{aligned} \tag{3}$$

Algorithm 1: `SCOPE` Entropy Weighted Ensembling

```
Require: input samples $\mathbf{X}_{\text{pen}}$ and $\mathbf{X}_{\text{ref}}$, trained models $M_{\text{pen}}$
    and $M_{\text{ref}}$, number of classes $m$.
Ensure: Final class prediction $y_{\text{ensemble}}$.
1: $\mathbf{Y}_{\text{pen}} \leftarrow M_{\text{pen}}(\mathbf{X}_{\text{pen}}), \quad \mathbf{Y}_{\text{ref}} \leftarrow M_{\text{ref}}(\mathbf{X}_{\text{ref}})$
2: Calculate $H_{\text{pen}}$ and $H_{\text{ref}}$ following Equation 4
3: $w_{\text{pen}} \leftarrow \sigma(H_{\text{pen}} - H_{\text{pen}}), \quad w_{\text{ref}} \leftarrow \sigma(H_{\text{pen}} - H_{\text{ref}})$
4: $\mathbf{Y}'_{\text{pen}} \leftarrow w_{\text{pen}} \cdot \mathbf{Y}_{\text{pen}}, \quad \mathbf{Y}'_{\text{ref}} \leftarrow w_{\text{ref}} \cdot \mathbf{Y}_{\text{ref}}$
5: $y_{\text{ensemble}} \leftarrow \arg\max(\mathbf{Y}'_{\text{pen}} + \mathbf{Y}'_{\text{ref}})$
6: return $y_{\text{ensemble}}$
```

By incorporating both path loss and phase shifts for different target distances ranging from 1 to 10 meters, SVA approximates distance scaling for CFR, aiding data augmentation to capture the effects of varying transmission distances in the near-field sub-THz band.

Antenna Gain Adjustment. In sub-THz systems, the received signal strength varies with the antenna gain, influenced by the angle of arrival. We collected real data using horn antennas with gains $G_0 = 20$ and 40 dBi. Additionally, assuming a near-zero incident angle in our setup, we applied a gain factor for data augmentation to simulate different scenarios, varying the transmit and receive antenna gains from 10 to 40 dBi. This selection represents a broad spectrum of realistic antenna configurations, enabling the model to generalize effectively across diverse propagation scenarios. By adjusting these gains, SVA captures signal strength variations for both penetrating and reflected signals. The gain-adjusted CFRs are $\text{CFR}_{\text{pen, gain}}(d) = \text{CFR}_{\text{pen}}(d) \cdot G_0, \quad \text{CFR}_{\text{ref, gain}}(d) = \text{CFR}_{\text{ref}}(d) \cdot G_0$.

C. Feature Extractor Architecture

The CNN-based feature extractor (Step V in Figure 1) entails three stacked convolutional blocks (`conv-block`) and a max-pooling (`MaxPool`) layer. Softmax is applied to the flattened output to obtain the probability distribution over the classes of materials. Each `conv-block` comprises two 2D convolutional layers with the same number of 3×3 kernels (filters) and a step size of 1, following the VGG design [9]. Specifically, we used 32, 64, and 128 filters, for the three `conv-block`.

D. Entropy Weighted Ensembling

The entropy-weighted ensembling method aims to dynamically balance the contributions of the penetrating model M_{pen} and reflected model M_{ref} based on their prediction confidence.

For an input sample $\mathbf{X}_{\text{pen}}$ or $\mathbf{X}_{\text{ref}}$, representing features obtained from the penetrating or reflected signals respectively, each model M_{pen} and M_{ref} produces a probability distribution over the m classes (line 1 of Algorithm 1). These distributions are represented as probability vectors $\mathbf{Y}_{\text{pen}} = [\mathbf{Y}_{\text{pen},1}, \mathbf{Y}_{\text{pen},2}, \ldots, \mathbf{Y}_{\text{pen},m}]$ and $\mathbf{Y}_{\text{ref}} = [\mathbf{Y}_{\text{ref},1}, \mathbf{Y}_{\text{ref},2}, \ldots, \mathbf{Y}_{\text{ref},m}]$, where each element $\mathbf{Y}_{\text{pen},j}$ and $\mathbf{Y}_{\text{ref},j}$ denotes the probability assigned by the penetrating or reflected model to class j, respectively. Hence, the entropy values H_{pen} and H_{ref} are calculated for each model's output distribution (line 2) and serve as a measure of the prediction

This article has been accepted for publication in IEEE Wireless Communications Letters. This is the author's version which has not been fully edited and content may change prior to final publication. Citation information: DOI 10.1109/LWC.2025.3576010

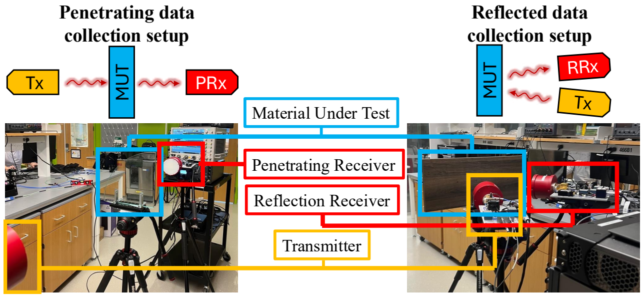

Fig. 2: Experimental setup with the TeraNova testbed for sub-THz material detection. The setup includes a transmitter (Tx), a penetrating receiver (PRx), and a reflection receiver (RRx). The material under test (MUT) is positioned between the transmitter and the penetrating receiver, while the reflection receiver captures reflected signals.

uncertainty of the penetrating and the reflected models. Mathematically, they are defined as

$$H_{\text{pen}} = -\sum_{j=1}^{m} \mathbf{Y}_{\text{pen},j} \log(\mathbf{Y}_{\text{pen},j});\ H_{\text{ref}} = -\sum_{j=1}^{m} \mathbf{Y}_{\text{ref},j} \log(\mathbf{Y}_{\text{ref},j}), \tag{4}$$

where lower values of H_{pen} and H_{ref} correspond to higher confidence. This entropy calculation is key to weighing each model's prediction based on its reliability for the specific input. Specifically, to determine the weights of the penetrating and reflected model—identified by w_{pen} and w_{ref} respectively—we set the entropy of the penetrating model, H_{pen}, as a reference. Next, each model's weight is calculated using the logistic sigmoid function (σ) applied to the entropy difference, i.e., $w_{\text{pen}} = \sigma(H_{\text{pen}} - H_{\text{pen}})$ and $w_{\text{ref}} = \sigma(H_{\text{pen}} - H_{\text{ref}})$ (line 3 of Algorithm 1). The sigmoid function effectively prioritizes models with lower entropy, assigning them higher weights. Thus, the entropy-weighted ensembling method adaptively balances M_{pen} and M_{ref} models based on their confidence, enhancing classification robustness. Each model's probability vector is then scaled by its corresponding weight to form a confidence-weighted distribution (line 4 of Algorithm 1):

$$\begin{aligned} \mathbf{Y}'_{\text{pen}} &= [w_{\text{pen}} \cdot \mathbf{Y}_{\text{pen},1}, w_{\text{pen}} \cdot \mathbf{Y}_{\text{pen},2}, \ldots, w_{\text{pen}} \cdot \mathbf{Y}_{\text{pen},m}] \\ \mathbf{Y}'_{\text{ref}} &= [w_{\text{ref}} \cdot \mathbf{Y}_{\text{ref},1}, w_{\text{ref}} \cdot \mathbf{Y}_{\text{ref},2}, \ldots, w_{\text{ref}} \cdot \mathbf{Y}_{\text{ref},m}], \end{aligned} \tag{5}$$

where each probability $\mathbf{Y}'_{\text{pen},j}$ and $\mathbf{Y}'_{\text{ref},j}$ is weighted according to the confidence-based factors w_{pen} and w_{ref}. This adjustment allows the more confident model to exert greater influence on the ensemble outcome. The final ensemble prediction y_{ensemble} is determined by selecting the class with the highest combined weighted probability (line 5 of Algorithm 1), i.e., $y_{\text{ensemble}} = \arg\max(\mathbf{Y}'_{\text{pen}} + \mathbf{Y}'_{\text{ref}})$ and each class probability is defined by $y_{\text{ensemble},j} = \arg\max(w_{\text{pen}} \cdot \mathbf{Y}_{\text{pen},j}, w_{\text{ref}} \cdot \mathbf{Y}_{\text{ref},j})$.

III. EXPERIMENTAL SETUP AND DATA COLLECTION

In this section, we describe the experimental setup for THz material detection using the TeraNova testbed [5], consisting of a transmitter (Tx), a penetrating receiver (PRx), and a reflection receiver (RRx), as shown in Figure 2. An LFM pulse is generated in MATLAB and converted to an analog signal via an Arbitrary Waveform Generator (AWG), capable of generating baseband (BB) or intermediate frequency (IF) signals up to 32 GHz. We generate a 1 μs pulse with 10 GHz IF bandwidth. The pulse is then upconverted to a 130 GHz passband signal by a THz RF front-end, with a transmit power of 13 dBm, ensuring sufficient signal strength for robust material classification while accounting for sub-THz propagation losses. At the receiver, an RF front-end downconverts the received passband signal, which is then captured by a Digital Storage Oscilloscope (DSO) with a 63.2 GHz operational bandwidth. The average noise floor of the setup is measured at –31 dBm, ensuring a sufficient signal-to-noise ratio (SNR) for accurate CFR estimation. The recorded signals undergo offline processing in MATLAB, including time synchronization and channel estimation, as detailed in Section II-A1.

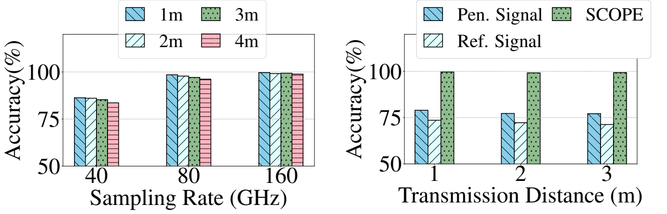

(a) Impact of sampling rate (b) Effect of transmission distance

Fig. 3: SCOPE performance illustrating (a) impact of sampling rates on accuracy at different transmission distances and (b) effect of transmission distances on accuracy for penetrating ('Pen.'), reflected ('Ref.'), and combined ('SCOPE') signals.

The material under test (MUT) is placed midway between the transmitter and the penetrating receiver. Tested materials include air (no material), metal, plastic, wood, and glass. While metal fully reflects the sub-THz signal, plastic, wood, and glass allow partial penetration and reflection. Transmission distances between the transmitter and receivers are set at 1, 2, 3, and 4 meters, with 40 dBi gain at both ends. Additional configurations with 40 dBi at the transmitter and 20 dBi at the receiver, as well as 20 dBi at both ends, are tested at a 2-meter distance. The half-power beamwidth (HPBW) of the antennas are 1.6 and 13 degrees respectively, ensuring directional transmission and reception, optimizing both penetrating and reflected signal capture.

IV. PERFORMANCE EVALUATION

The classification of materials such as air, wood, plastic, glass, and metal is central to evaluating SCOPE 's performance, as their unique material-level properties significantly influence sub-THz signal interactions. Factors such as density, electromagnetic characteristics, and surface structure determine how signals penetrate, reflect, and scatter, directly impacting detection accuracy. Air serves as a baseline with minimal interaction, while wood and plastic, with moderate density and partial transparency, challenge the system due to subtle distortions from partial penetration and reflection. Glass introduces strong reflection with partial penetration, and metal, being fully reflective, poses the most stringent challenge. Evaluating these materials highlights the system's ability to adapt to diverse material properties.

A. *Performance of SCOPE at Different Sampling Frequencies*

We evaluate SCOPE's material classification accuracy on data sampled at various rates across different transmission distances to analyze the impact of sampling frequency. Figure 3a illustrates how accuracy improves with higher sampling rates

This article has been accepted for publication in IEEE Wireless Communications Letters. This is the author's version which has not been fully edited and content may change prior to final publication. Citation information: DOI 10.1109/LWC.2025.3576010

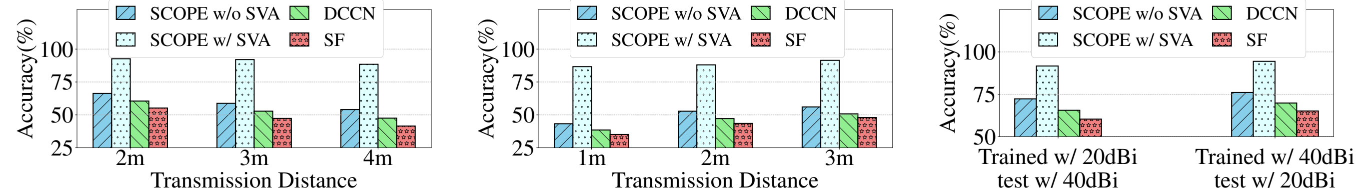

(a) Trained with data from 1 m of transmission distance, tested with others.

(b) Trained with data from 4 m of transmission distance, tested with others.

(c) Trained with one transmit antenna gain, tested with others.

Fig. 4: Performance comparison of `SCOPE` in generalizing across transmission distances and transmit antenna gains

of 40 GHz, 80 GHz, and 160 GHz, tested at distances of 1, 2, 3, and 4 meters. The results demonstrate that higher sampling frequencies substantially enhance accuracy, particularly at greater distances. For example, at a sampling rate of 40 GHz, accuracy drops from 86.29% at 1 m to 83.60% at 4 m, whereas at 160 GHz, accuracy remains consistently high, achieving 99.66% at 1 m and 98.88% at 4 m.

B. Evaluating `SCOPE`'s Entropy-Weighted Ensembling

Figure 3b compares material detection performance using three information sources: (i) the penetrating signal alone, (ii) the reflected signal alone, and (iii) the combination of both signals through `SCOPE`'s entropy-weighted ensembling method. The results clearly demonstrate the superiority of the proposed ensembling approach. Using the penetrating signal alone allows achieving accuracies of 78.98% at 1 m, which decreases to 77.12% at 3 m, while the reflected signal provides 73.60% accuracy at 1 m, which drops to 71.29% at 3 m. Instead, `SCOPE`'s entropy-weighted ensembling achieves consistently high accuracy, exceeding 99% across distances from 1 to 3 meters. These results indicate that by dynamically balancing the contributions of the penetrating and reflected signals based on their confidence levels, the entropy-weighted ensembling approach allows performing accurate material classification under varying transmission conditions.

C. Generalization Performance of `SCOPE`

Figure 4 highlights the critical role of SVA in enabling `SCOPE` to generalize across transmission distances and antenna gains. The selected distances (1—4 meters) represent a practical near-field range for sub-THz systems, capturing meaningful signal variations while balancing experimental feasibility. In Figure 4a, the model trained on data from 1 meter distance exhibits a substantial drop in accuracy when tested on data from 2–4 meters distance without applying SVA, reaching as low as 54.05% at 4 meters. In contrast, by applying SVA, `SCOPE` improves performance, boosting accuracy to 88.43%—a relative improvement of up to 63.6%. Competing methods such as DCNN [2] and SF [3], which rely solely on reflected signals, perform worse under the same conditions, achieving only 47.5% and 41.5% accuracy at 4 meters, respectively. Similarly, in Figure 4b, when trained on 4-meter data and tested on other distances, the results follow a similar trend, further underscoring SVA's importance for robust generalization.

Figure 4c evaluates generalization across antenna gains, where the model is trained with one gain (e.g., 20 dBi) and tested with another (e.g., 40 dBi), and vice versa. Without SVA, significant accuracy degradation occurs, while SVA improves accuracy by 24-–27%. Comparatively, DCNN [2] and SF [3] experience even sharper declines, achieving only 65.5% and 60.3% accuracy, respectively, when tested across different antenna gains.

While `SCOPE` demonstrates robust generalization across varying distances and antenna gains, evaluations were conducted within the range of 1–4 meters and with antenna gains of 20 dBi and 40 dBi. These configurations represent typical sub-THz systems but they may not fully capture extreme long-range scenarios or hardware setups with significantly different antenna gains. Additionally, `SCOPE`'s performance in highly dynamic environments with rapidly changing channel conditions requires further investigations.

V. CONCLUSIONS

This letter presents `SCOPE`, a robust sub-THz cooperative sensing system that employs entropy-weighted ensembling and SVA to achieve high-accuracy material detection by generalizing across different transmission distances and antenna gains. It adaptively balances the contributions of penetrating and reflected signals by weighting them according to the confidence of the CNN-based material predictions. Experimental evaluations with the TeraNova testbed show that `SCOPE` achieves up to 99% accuracy when trained and tested with the same transmission distance and antenna gains, and up to 94% accuracy when generalizing across different distances and transmission antenna gains.

REFERENCES

[1] S. Skaria, N. Hendy, and A. Al-Hourani, "Machine-Learning Methods for Material Identification Using mmWave Radar Sensor," *IEEE Sensors Journal*, vol. 23, no. 2, pp. 1471–1478, 2022.

[2] J. Weiß and A. Santra, "Material Classification Using 60-GHz Radar and Deep Convolutional Neural Network," in *2019 International Radar Conference (RADAR)*. IEEE, 2019, pp. 1–6.

[3] S. He, Y. Qian, H. Zhang, G. Zhang, M. Xu, L. Fu, X. Cheng, H. Wang, and P. Hu, "Accurate Contact-free Material Recognition with Millimeter Wave and Machine Learning," in *International Conference on Wireless Algorithms, Systems, and Applications*. Springer, 2022, pp. 609–620.

[4] R. N. Khushaba and A. J. Hill, "Radar-based Materials Classification using Deep Wavelet Scattering Transform: A Comparison of Centimeter vs. Millimeter Wave Units," *IEEE Robotics and Automation Letters*, vol. 7, no. 2, pp. 2016–2022, 2022.

[5] P. Sen, D. A. Pados, S. N. Batalama, E. Einarsson, J. P. Bird, and J. M. Jornet, "The TeraNova Platform: An Integrated Testbed for Ultra-Broadband Wireless Communications at True Terahertz Frequencies," *Computer Networks*, vol. 179, p. 107370, 2020.

[6] Z. Wen, M. Liu, Y. Chen, N. Zhao, A. Nallanathan, and X. Yang, "Multi-Component LFM Signal Parameter Estimation for Symbiotic Chirp-UWB Radio Systems," *IEEE Transactions on Cognitive Communications and Networking*, 2024.

[7] P. Sen, H. Pandey, and J. M. Jornet, "Ultra-Broadband Chirp Spread Spectrum Communication in the Terahertz Band," in *Next-generation spectroscopic technologies XIII*, vol. 11390. SPIE, 2020, pp. 7–18.

[8] P. Sen, S. Badran, V. Petrov, A. Singh, and J. M. Jornet, "Impact of the Antenna on the Sub-Terahertz Indoor Channel Characteristics: An Experimental Approach," in *ICC 2024 - IEEE International Conference on Communications*, 2024, pp. 2537–2542.

[9] K. Simonyan and A. Zisserman, "Very deep convolutional networks for large-scale image recognition," *arXiv preprint arXiv:1409.1556*, 2014.